Minimally Invasive Microelectrode Biosensors Based on Platinized Carbon Fibers for in Vivo Brain Monitoring

Charles Chatard, Andrei Sabac, Laura Moreno-Velasquez, Anne Meiller, Stéphane Marinesco

ACS central science

Research Article

Cite This: ACS Cent. Sci. 2018, 4, 1751−1760

http://pubs.acs.org/journal/acscii

Minimally Invasive Microelectrode Biosensors Based on Platinized Carbon Fibers for *in Vivo* Brain Monitoring

Charles Chatard,[†,‡,⊥,#] Andrei Sabac,[§,∥,⊥] Laura Moreno-Velasquez,[†,#] Anne Meiller,[‡,#] and Stephane Marinesco*[,†,‡,#]

[†]INSERM U1028, CNRS UMR5292, Team TIGER, Lyon Neuroscience Research Center—CRNL, Lyon 69373 Cedex 08, France

[‡]AniRA—Neurochem Technological Platform, 8 Avenue Rockefeller, Lyon 69373 Cedex 08, France

[§]CNRS UMR5270, Lyon Nanotechnologies Institute—INL, Villeurbanne 69621, France

[∥]CNRS UMR5005, Ampère Laboratory, Villeurbanne 69621, France

[⊥]INSA de Lyon, Villeurbanne 69100, France

[#]Université Claude Bernard Lyon 1, Lyon 69100, France

Supporting Information

ABSTRACT: The ability to monitor the chemical composition of brain interstitial fluid remains an important challenge in the field of bioanalytical chemistry. In particular, microelectrode biosensors are a promising resource for the detection of neurochemicals in interstitial fluid in both animals and humans. These biosensors can provide second-by-second temporal resolution and enzymatic recognition of virtually any redox or nonredox molecule. However, despite miniaturization of these sensors to 50−250 μm in diameter to avoid vascular and cellular injury, inflammation and foreign-body reactions still occur following their implantation. Here, we fabricated microelectrodes with platinized carbon fibers to create biosensors that have an external diameter that is less than 15 μm. Platinization was achieved with physical vapor deposition, and increased sensitivity to hydrogen peroxide and improved enzymatic detection were observed for these carbon fiber microelectrodes. When these devices were implanted in the brains of rats, no injuries to the parenchyma or brain blood vessels were detected. In addition, these microelectrodes provided different estimates of basal glucose, lactate, and oxygen concentrations compared to conventional biosensors. Induction of spreading depolarization in the cerebral cortex further demonstrated the greater sensitivity of our microelectrodes to dynamic neurochemical changes. Thus, these minimally invasive devices represent a major advance in our ability to analyze brain interstitial fluid.

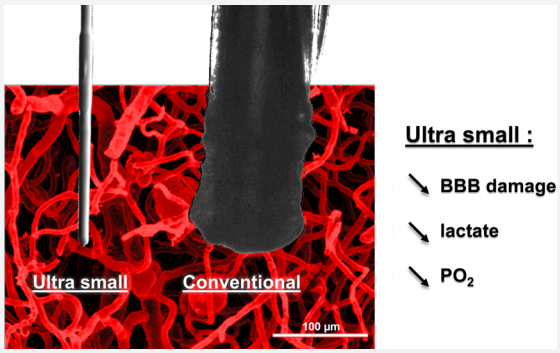

INTRODUCTION

Analyses of brain interstitial fluid can reveal important neurochemical information about the pathophysiological state of the brain. In the clinic or in laboratory animals, the ability to detect extracellular concentrations of brain energy metabolites such as glucose, lactate, and pyruvate over time can help detect specific patterns of brain injury.[1] In addition, activation of neuronal networks that lead to a synaptic or extrasynaptic release of neurotransmitters can be detected in interstitial fluid. Estimates of extracellular concentrations of neurochemicals that are provided by implantable devices, such as microdialysis probes or microelectrodes, are usually more accurate than those obtained with optical or spectroscopic techniques. However, probe size and local injury due to implantation are key parameters for obtaining reliable measurements *in vivo*.[2] In particular, rupture of brain capillaries during probe implantation represents a major trigger for inflammation and a foreign-body response.[3]

The ability to construct carbon fiber microelectrodes to detect electroactive neurotransmitters has significantly contributed to our understanding of the dopamine system and its implications in regard to reward and addiction conditions.[4−8] In particular, the small diameter of these microelectrodes (approximately 7 μm) makes them suitable for interstitial fluid analyses. However, electrochemical analysis using carbon fiber microelectrodes is currently limited to the detection of endogenous redox molecules such as dopamine or serotonin.[4] Microelectrode biosensors can extend the range of molecules amenable to electrochemical detection by using oxidase enzymes for molecular recognition of nonredox neurotransmitters and metabolites. Typically, oxidases oxidize their substrate while consuming O_2 and producing hydrogen peroxide (H_2O_2). Hence, most microelectrode biosensors for brain analysis are based on platinum (Pt) electrodes that

Received: October 30, 2018
Published: December 14, 2018

DOI: 10.1021/acscentsci.8b00797
ACS Cent. Sci. 2018, 4, 1751−1760

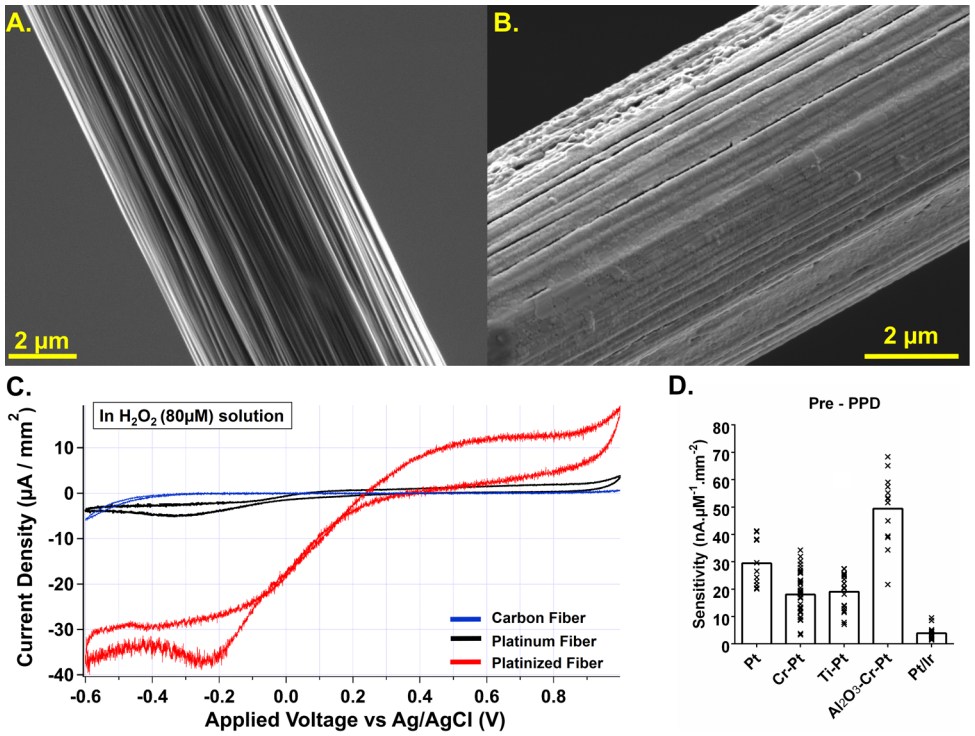

Figure 1. Surface and electrochemical properties of platinized carbon fibers. Electron microscopy images of (A) a bare 7 μm diameter carbon fiber (HV, 2 kV; magnitude, 18.7 kx; WD, 8.94 mm) and (B) a carbon fiber with Ti and Pt applied by evaporation (HV, 5 kV; magnitude, 26.9 kx; WD, 9.27 mm). A rough Pt surface is observed in the latter. (C) Representative cyclic voltammograms obtained in 80 μM H_2O_2/0.01 M PBS (pH 7.4) under ambient air for a bare carbon fiber (7 μm diameter, blue trace), a platinized carbon fiber (7 μm diameter, red trace), and a platinum−iridium fiber (75 μm diameter, blue trace). A lower potential for H_2O_2 oxidation and reduction is observed for the platinized carbon fiber, as well as a high current density. (D) H_2O_2 sensitivities of platinized carbon fibers with Cr, Ti, and Al_2O_3−Cr as adhesion layer, or without adhesion layer (before PPD functionalization). Bars represent the mean, and x individual microelectrodes.

monitor H_2O_2 produced by an enzyme. Unfortunately, the size of these Pt microelectrodes is quite large, on the order of 50−250 μm. As a result, their implantation in brain parenchyma can injure blood vessels, cause diffusion of serum albumin and monocytes into brain tissue, and initiate an inflammatory reaction that can lead to a foreign-body reaction.[3] Over an extended period of time, these reactions can have disastrous consequences. However, even within the first hour after implantation, local brain tissue neurochemistry can be affected.

In general, carbon is poorly suited for H_2O_2 oxidation. However, electrodeposition of Pt on the surface of carbon fibers has been performed to obtain microelectrodes that are sensitive to H_2O_2.[9−11] Unfortunately, the lifetime of such Pt deposits is usually only a few hours. Alternatively, Pt can be readily deposited on large silicon or ceramic planar surfaces by using a physical vapor deposition method. To date, such processes have undergone only limited testing on smaller cylindrical-shaped objects. Therefore, here we examined the feasibility of platinizing 7 μm diameter carbon fibers with physical vapor deposition to obtain minimally invasive microelectrode biosensors. We tested these devices *in vivo* to examine their ability to detect O_2, glucose, and lactate in brain tissues. In addition, we examined the ability of these smaller probes to measure extracellular concentrations of neurochemicals in brain tissue. The neurochemical data obtained were compared with the data obtained with conventional platinum wire microelectrodes (80−90 μm diameter). We also characterized the response of our smaller microelectrode biosensors to spreading depolarization (SD) in the cortex. SDs are waves of nearly complete depolarization of neurons and glial cells that travel through the cortex at a typical speed of 2−4 mm min^{-1}.[12] This phenomenon induces massive metabolic demand in brain tissue, which is correspondingly accompanied by rapid changes in oxygen, glucose, and lactate concentrations. The latter provides an ideal physiological condition under which to test the *in vivo* performance of bioanalytical devices.[13]

RESULTS AND DISCUSSION

Carbon Fiber Platinization. For the improvement of the sensitivity of H_2O_2 detection by carbon fibers, a 100 nm platinum (Pt) catalytic layer was deposited onto carbon fibers using evaporation deposition. For carbon fiber platinization, different materials were evaluated for their capacity to provide an adhesion layer prior to deposition of Pt. These materials included titanium (Ti; n = 19), chromium (Cr; n = 47), and aluminum oxide (Al_2O_3/Cr; n = 13). On some carbon fibers, the adhesion layer was omitted (n = 11). Scanning electron microscopy showed that all these methods allowed a successful deposition of Pt. The platinized carbon fibers exhibited a uniform Pt layer that fitted the underlying striate structure of the original carbon fiber (Figure 1A). This layer was stable and was observed several days after platinization. Moreover, platinization via physical vapor deposition created a rough Pt surface with a potentially larger active surface than that of solid Pt/iridium (Ir) wires (Figure 1B,C).

Electrochemical Properties. These Pt surfaces were subsequently tested electrochemically by cyclic voltammetry in an 80 μM H_2O_2 solution (−0.2 to 1.0 V versus Ag/AgCl, 100

DOI: 10.1021/acscentsci.8b00797
ACS Cent. Sci. 2018, 4, 1751−1760

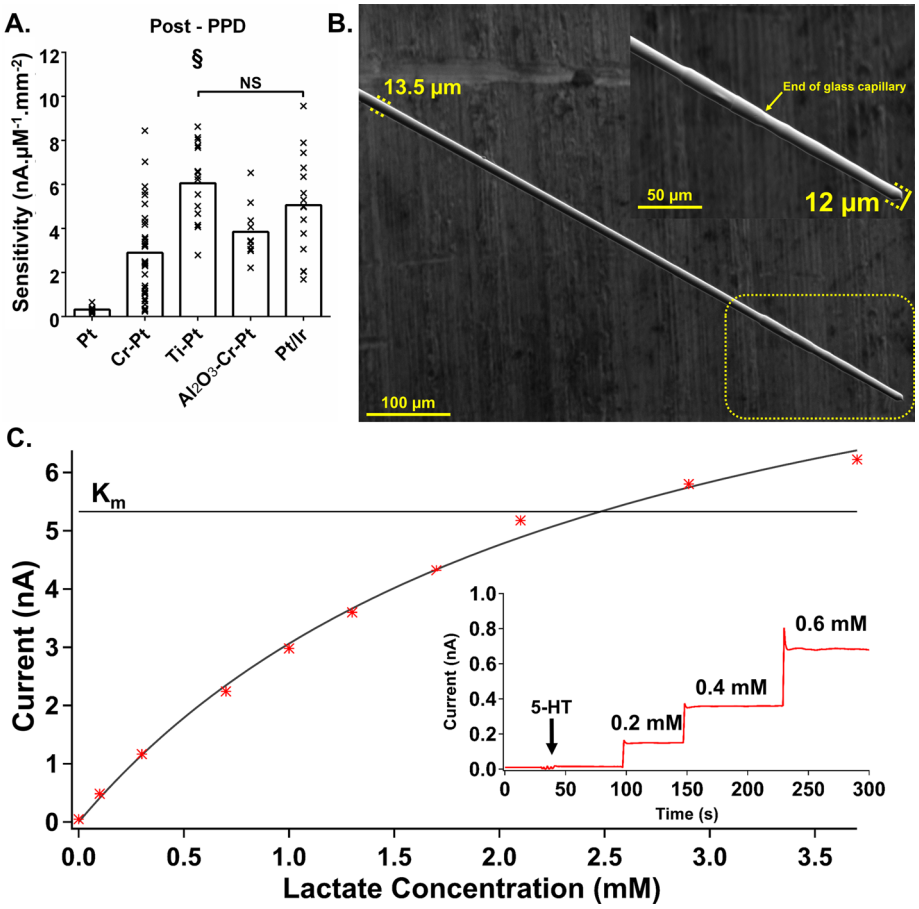

Figure 2. Biofunctionalization and calibration. (A) H_2O_2 sensitivities of batches of microelectrodes after PPD functionalization, showing the dramatic decrease in H_2O_2 at platinized carbon fibers but not solid Pt/Ir wires. (B) Electronic microscopy image of a small microelectrode biofunctionalized with a lactate oxidase enzyme and PPD layers (HV, 1 kV; magnitude, 421 x; WD, 19.57 mm). Inset shows an enlargement of the sensing part of the biosensor with a 12 μm external diameter (HV, 1 kV; magnitude, 1.26 kx; WD, 19.57 mm). (C) Current−concentration relationship and Michaelis−Menten fit for the lactate biosensor. Inset shows a calibration example with the selectivity test showing no detection of serotonin (5-HT) and subsequent 0.2 mM steps in lactate concentration in a 0.01 M PBS (pH 7.4) solution. Bars represent the mean, and *x* individual microelectrodes; NS, not significant; §, significant difference (one-way ANOVA with Tukey's posthoc test, $P < 0.0001$, $F = 17.9$, $R = 0.46$).

mV s^{-1}). The bare carbon fibers yielded very small H_2O_2 redox currents, with H_2O_2 oxidation occurring at holding potentials greater than 0.8 V, and no reduction current detected in this potential range (Figure 1C). In contrast, the solid Pt/Ir wires exhibited clear H_2O_2 oxidation above 0.2 V and reduction below 0.2 V, consistent with previous reports.[10,14] Cyclic voltammograms obtained for the platinized carbon fibers showed a similar redox pattern to the solid Pt/Ir wires, and consistently with the higher H_2O_2 sensitivity, the H_2O_2 redox currents were higher for the former (Figure 1C and Figure S1).

For platinized carbon fibers, the sensitivities of the resulting microelectrodes to H_2O_2 significantly differed depending on the material used as an adhesion layer (expressed as mean ± standard deviation in all *in vitro* experiments: [Pt, 29.4 ± 8.5 nA μM^{-1} mm^{-2}], [Cr−Pt, 18.0 ± 7.0 nA μM^{-1} mm^{-2}], [Ti−Pt, 19.0 ± 6.7 nA μM^{-1} mm^{-2}], and [Al_2O_3−Cr−Pt, 49.4 ± 13.1 nA μM^{-1} mm^{-2}]). Platinized carbon fiber microelectrodes exhibited sensitivity to H_2O_2 that was greater than that of the solid Pt/Ir wire electrodes (4.37 ± 2.78 nA μM^{-1} mm^{-2}; $n = 10$; one-way ANOVA with Tukey's posthoc test, $P < 0.0001$, $F = 67.6$, $R = 0.732$; Figure 1D). In subsequent experiments, platinized carbon fibers with sensitivities less than 7 nA μM^{-1} mm^{-2} were excluded, and these represented 17% of the fabricated electrodes.

Therefore, carbon fiber platinization by physical vapor deposition improved its catalytic activity toward H_2O_2 oxidation. Pt deposition is a commonly used technique in the field of biomedical micro-electromechanical systems (bioMEMs) technology, but it is usually performed with flat silicon substrates.[15] Our results show that, despite their unusual cylindrical geometry, carbon fibers could be successfully covered with a uniform Pt layer, and the sensitivity achieved was similar or better than the sensitivity exhibited in parallel by commercially available solid Pt wires.

Biofunctionalization. The platinized carbon fibers were next functionalized with an electropolymerized layer of poly *m*-phenylenediamine (PPD) to block nonspecific oxidation of endogenous molecules such as ascorbic acid or dopamine,[16,17] followed by enzyme immobilization using poly(ethylene glycol) diglycidyl ether (PEGDE) cross-linking (see methods, Supporting Information). Sensitivity to H_2O_2 decreased dramatically after functionalization of the electrodes with PPD. The platinized carbon fibers with no adhesion layer lost almost all of their sensitivity to H_2O_2 (−98.8 ± 0.5%), while the fibers including an adhesion layer exhibited a 63−92% loss

DOI: 10.1021/acscentsci.8b00797
ACS Cent. Sci. 2018, 4, 1751−1760

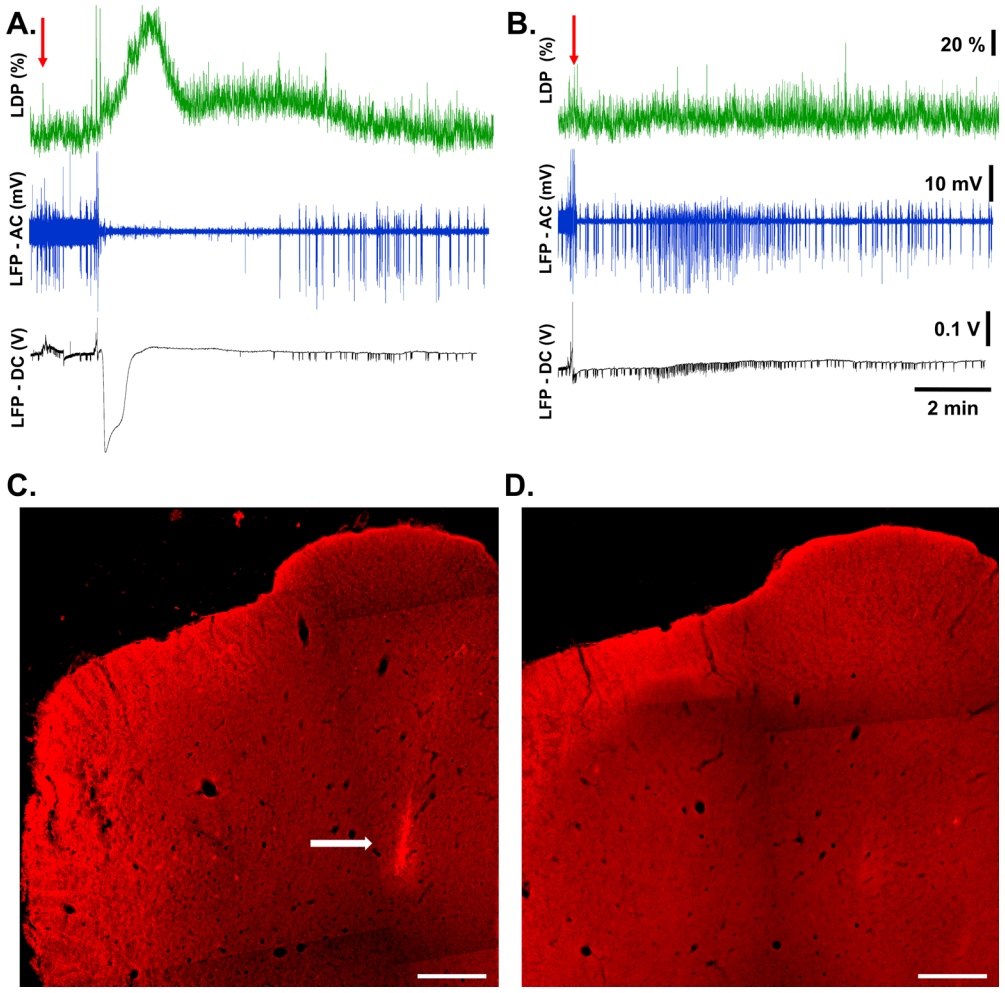

Figure 3. Evaluation of the physiological impact of biosensor implantation. Laser Doppler responses (green traces) and AC (blue traces) and DC (black traces) electrocorticographic responses to (A) large biosensors with an 80−90 μm outer diameter and (B) small biosensors (n = 3). SD was evoked by implantation (indicated with a red arrow) of the large biosensor, but not for implantation of the small biosensor. BBB integrity was assessed with Evans Blue dye 2 h after implantation of (C) a 250 μm diameter commercial optic fiber and (D) a small microelectrode in the frontal cortex. BBB disruption was observed around the commercial optic fiber (indicated with a white arrow), but not around the small microelectrode. White scale bar, 0.5 mm.

in H_2O_2 sensitivity ([Cr−Pt, 83.3 ± 12.7%], [Ti−Pt, 62.7 ± 17.9%], and [Al_2O_3−Cr−Pt, 91.7 ± 1.9%]; P < 0.0001, n = 16; Figure 2A). Eventually the Pt deposition procedure with the highest sensitivity to H_2O_2 after PPD functionalization included application of a 15 nm Ti adhesion layer and a 100 nm Pt layer. These fibers only exhibited a 64 ± 17% loss in sensitivity and a final sensitivity to H_2O_2 of 6.06 ± 1.72 nA μM^{-1} mm^{-2} (n = 16). This sensitivity was significantly superior to the other platinization procedures (one-way ANOVA with Tukey's posthoc test, P < 0.0001, F = 17.9, R = 0.460). In contrast, the microelectrodes based on solid commercial Pt wires did not exhibit a decrease in sensitivity (+11 ± 22%, P = 0.806, n = 10). H_2O_2 detection limits after functionalization with PPD were 10.2 ± 2.9 nM (Ti−Pt carbon fiber) and 16.7 ± 13.7 nM (solid Pt/Ir, 3 times the standard deviation of *in vitro* noise; n = 6). Thus, H_2O_2 detection after functionalization with PPD did not significantly differ between the platinized carbon fibers and the commercial Pt wires (4.67 ± 2.65 nA μM^{-1} mm^{-2}) (P = 0.118).

Throughout the rest of the study, carbon fibers with a 15 nm Ti adhesion layer and a 100-Pt layer deposited by evaporation were therefore chosen for their superior electrochemical performance. They also exhibited excellent sensitivity to O_2 reduction (0.096 ± 0.026 pA $mmHg^{-1}$ μM^{-2}), with a limit of detection of 0.1 ± 0.02 mmHg (n = 5). These microelectrodes were also tested after 6 months of storage (room temperature in the dark) and exhibited similar sensitivity to H_2O_2 compared to initial tests (before, 16.6 ± 6.2 nA μM^{-1} mm^{-2}; 6 month, 15.8 ± 8.3 nA μM^{-1} mm^{-2}; parametric Student's t test, n = 17, P = 0.73).

The microelectrodes were further functionalized with enzyme immobilization, and layers of polyurethane were added to increase the linear range of the biosensors.[18] These functional layers were approximately 2−3 μm thick, and the resulting microelectrode biosensors had an average external diameter of 11−13 μm (Figure 2B). *In vitro* calibrations revealed a typical current−concentration relationship that followed Michaelis−Menten-like kinetics characterized by an initial linear range and a plateau (e.g., lactate calibration as shown in Figure 2C). The small glucose biosensors exhibited a sensitivity of 0.55 ± 0.21 nA μM^{-1} mm^{-2}, a limit of detection of 3.08 ± 0.88 μM, and an apparent K_m, K_m^{app}, of 4.49 ± 1.28 mM (n = 7). For the lactate biosensors, their sensitivity was 0.20 ± 0.04 nA μM^{-1} mm^{-2}, with a limit of

DOI: 10.1021/acscentsci.8b00797
ACS Cent. Sci. 2018, 4, 1751−1760

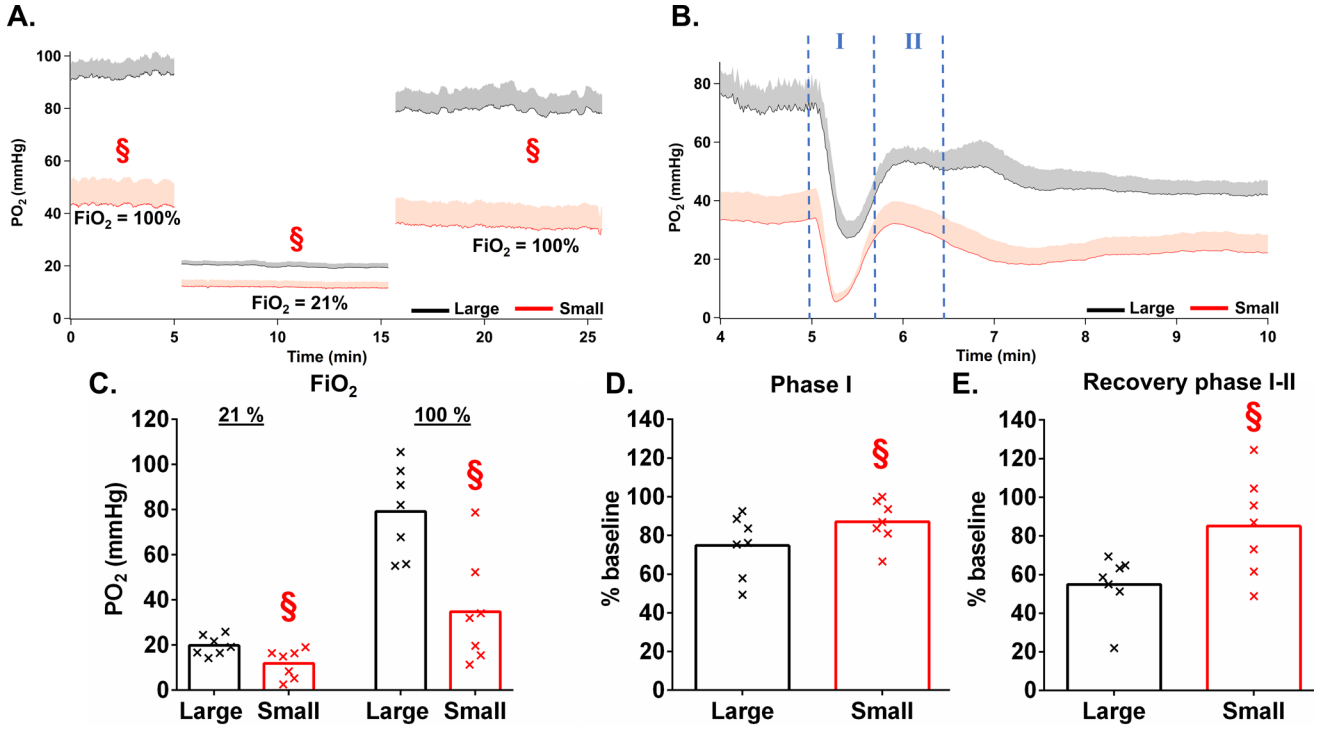

Figure 4. PO_2 monitoring. *In vivo* monitoring of basal PO_2: (A) under 21% and 100% fraction of inspired O_2 (FiO_2) and (B) during SD induction in the cortex. PO_2 responses to SD are analyzed in two distinct phases that are separated by dashed blue lines. The small microelectrodes (7 μm diameter; red trace) detected lower PO_2 levels ($P_{100\%}$ = 0.002, $P_{21\%}$ = 0.045, and $P_{100\%}$ = 0.001) than the larger commercial optic fibers (250 μm diameter; black trace). The mean values are represented by a solid line, and SEM is represented with light color shading. (C) Mean basal PO_2 level detected by the two sets of biosensors under 100% and 21% FiO_2. (D) Percentage decrease in PO_2 during the initial phase of the PO_2 response to SD (phase I). (E) Percentage PO_2 recovery from phase I to II (% of initial baseline PO_2). (Bars represent the mean values, and x individual experiments; §, significant difference, $P < 0.05$.)

detection of 1.16 ± 0.26 μM, and a K_m^{app} of 2.60 ± 1.13 mM. We also constructed more conventional biosensors composed of 75 μm diameter commercial solid Pt/Ir wires that had a final external diameter of 80−90 μm. These larger biosensors displayed similar Michaelis−Menten kinetics and K_m^{app} values, yet had slightly lower sensitivities (0.26 ± 0.11 nA μM^{-1} mm^{-2} for glucose [P = 0.007, n = 7] and 0.14 ± 0.03 nA μM^{-1} mm^{-2} for lactate [P = 0.01, n = 7]). For O_2 detection, the platinized carbon fiber electrodes were simply coated with Nafion to protect them from *in vivo* biofouling. Overall, the platinized carbon fibers allowed the fabrication of minimally invasive microelectrode biosensors that were less than 15 μm in diameter, which is smaller than the average distance between brain capillaries.[19,20]

Implantation Impact. When a probe is implanted in the brain, this can lead to tissue strain, tearing and shearing of the extracellular matrix, and disruption of cellular processes and the blood−brain barrier (BBB).[3] The immediate effect of implantation of conventional microelectrode biosensors with 80−90 μm diameter was deformation of the brain surface, including rupture of the pial surface and parenchyma at the site of implantation (Video S1). This type of mechanical stimulation of the brain surface typically leads to cortical SD. When we performed implantations of our minimally invasive microelectrode biosensors, we did not provoke any deformation of the brain surface, and the biosensors entered the parenchyma smoothly (Video S2). Direct current electrocorticography and laser Doppler flowmetry were used to detect SD following implantation in three anesthetized animals. For the conventional 80−90 μm diameter microelectrode biosensors, implantation was followed by a large depolarization potential that lasted less than a minute. This response was coupled to a wave of spreading depression of neuronal activity that lasted approximately 5 min, and to a hyperemic wave that induced an 85% increase in regional cerebral blood flow (Figure 3A). In contrast, these neurophysiological events were not detected when we implanted our small microelectrode biosensors, indicating that cortical SD was not induced (Figure 3A).

For the evaluation of BBB integrity, an intraperitoneal injection of Evans Blue dye was performed. This dye binds serum albumin and can diffuse into the brain parenchyma if the BBB is compromised.[21] Because it fluoresces at 680 nm,[22] it can be directly observed by fluorescence microscopy (see methods, Supporting Information). Evans Blue staining revealed disruption of the BBB around the implantation site of a commercial 250 μm diameter oxygen sensor (arrow on bright red stripe, Figure 3C), whereas no staining was observed at the implantation sites of our small microelectrodes (Figure 3D). On the basis of the absence of gross BBB disruption and SD generation upon implantation of our minimally invasive microelectrode biosensors, it appears that these biosensors are less disruptive of brain parenchyma compared to conventional devices, and this is important for efficacy of monitoring by these biosensors.

***In Vivo* Monitoring.** *Oxygen.* Basal partial pressure of oxygen (PO_2) was detected in the cortex of anesthetized rats by a small microelectrode (platinized carbon fiber) and by a commercially available optical oxygen probe with an outer diameter of 250 μm. There was 1−2 mm between the

DOI: 10.1021/acscentsci.8b00797
ACS Cent. Sci. 2018, 4, 1751−1760

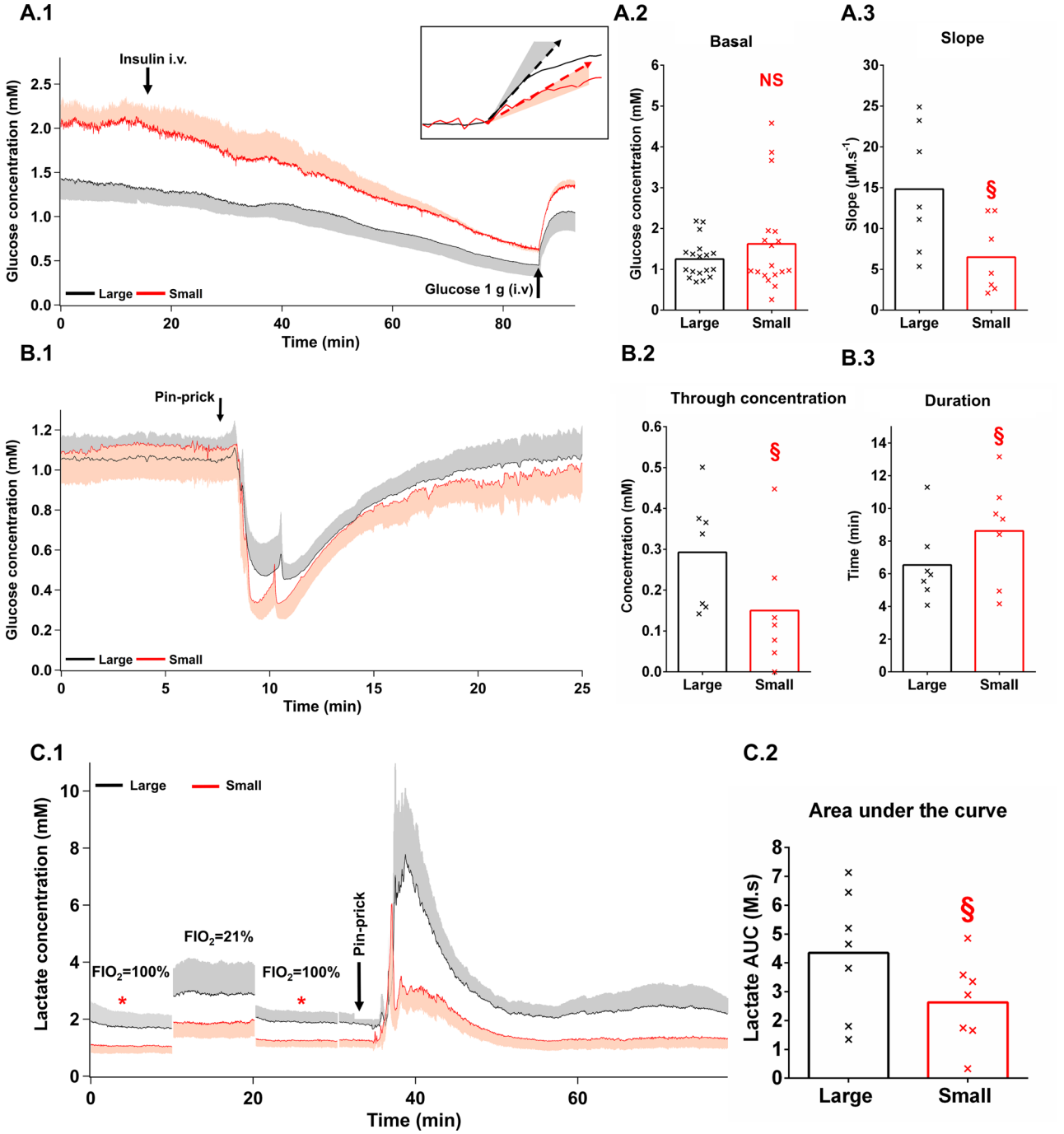

Figure 5. *In vivo* detection of brain glucose and lactate. Parallel detection of glucose with large biosensors (80−90 μm diameter; black trace) and small biosensors (12−15 μm diameter; red trace) after an intravenous injection of insulin followed by(A1) an injection of 1 mmol of glucose and (B1) SD induction in the cortex. The inset of part A1 shows glucose slope after the glucose injection. The mean is represented by a solid line, and SEM is represented with light color shading. (A2) Mean basal extracellular glucose concentrations detected over 5 min prior to the injection of insulin. (A3) Mean slope of glucose extracellular concentration after the intravenous injection of glucose. (B2) Trough concentration of glucose after SD induction. (B3) Duration of glucose recovery to 80% of baseline concentration. (C1) Basal levels of lactate detected under conditions of 21% FiO_2 and 100% FiO_2, and then following induction of SD (the 5 min period of stabilization after changes in FiO_2 were made was removed). (C2) Area under the curve was calculated for 20 min after SD. Significantly smaller concentrations were detected by the small microelectrodes (P = 0.029). (Bars represent the mean, and x individual experiments; §, significant difference, $P < 0.05$; NS, not significant.)

implanted sensors, and measurements were made following a change in the fraction of inspired oxygen (FiO_2) from 100% (pure oxygen) to 21% (ambient air) and back to 100% (Figure 4A). The readings of PO_2 by the small microelectrodes were consistently lower (expressed as mean ± standard error of the mean in all *in vivo* experiments: 43.2 ± 0.2, 11.9 ± 0.1, and 34.8 ± 0.3 mmHg, respectively) compared to those of the larger optic fiber probes (92.3 ± 0.4, 19.8 ± 0.2, and 79.2 ± 0.4 mmHg, respectively). These measured differences were also significant under all three conditions (P = 0.002, P = 0.045, and P = 0.001, respectively; n = 7) (Figure 4C). Moreover, the PO_2 values obtained with

DOI: 10.1021/acscentsci.8b00797
ACS Cent. Sci. 2018, 4, 1751−1760

the large commercial probes were consistent with those measured by Ledo et al.[23] in freely behaving rats that were implanted with silicon probes of similar size.

To test the response of our sensors to rapid transient changes in PO_2, we induced SD in the cortex. This depolarization event induces a multiphasic response which is initially characterized by a sharp decrease in PO_2 (phase I), which corresponds to the large metabolic demand generated by depolarization, followed by an increase in PO_2 (phase II), which is related to vasodilation of brain capillaries.[24,25] The initial PO_2 decrease (Figure 4B, phase I) was detected as a sharper change by the small microelectrodes compared with the optic fiber sensors, with the percent decreases from baseline to the trough of the response detected as 87.1 ± 4.3% and 74.8 ± 6.0%, respectively (P = 0.001; n = 7) (Figure 4D). Then, the recovery of PO_2 toward its initial value (phase II) was detected as being faster and larger with the smaller probes, with the percent increases in PO_2 from baseline detected as 85.1 ± 9.8% and 54.9 ± 5.9%, respectively (P = 0.003; n = 7; Figure 4E). Finally, PO_2 was detected as returning to its initial baseline level during phase II according to the smaller probes (98 ± 22% of baseline), whereas PO_2 was detected below its initial level when measured by the larger optic fibers (80 ± 10% of baseline). Thus, the minimally invasive microelectrodes detected sharper and larger changes in PO_2 in response to SD compared to the larger probes.

Glucose. Enzyme biosensors prepared from our small microelectrodes were compared *in vivo* with larger biosensors (80−90 μm external diameter) in the detection of glucose and lactate in anesthetized animals. For glucose detection, (1) the extracellular concentration of basal glucose, (2) glucose diffusion across the BBB (Figure 5A1), and (3) rapid transient changes in glucose level evoked by SD (Figure 5B1) were detected. One hour after the probes were implanted, both sets of biosensors detected similarly stable glucose levels in the cortex, although a nonsignificant trend for detecting lower glucose levels was observed with the small biosensors (1.62 ± 0.29 mM versus 1.25 ± 0.11 mM, respectively; P = 0.246; n = 18) (Figure 5A2). Next, the glucose diffusion rate across the BBB was measured. Briefly, blood glucose was first lowered by an injection of insulin (50 U kg^{-1}) to 35−40 mg dL^{-1}. Meanwhile, the interstitial level of brain glucose decreased to 32% of its initial value. A subsequent intravenous injection of 1 mmol of glucose evoked a rapid increase in brain interstitial glucose, and the slope of this increase was detected as 14.8 ± 2.9 μM s^{-1} by the large biosensors and 6.50 ± 1.68 μM s^{-1} by the small biosensors (P = 0.01; n = 7) (Figure 5A3). We hypothesize that this faster increase reflects local disruption of the BBB around the large biosensors, and images from the Evans Blue staining experiments described above support this hypothesis.

Consistent with previous data,[23] a decrease in glucose in response to SD was detected by the small biosensors and the larger glucose biosensors. However, the minimal glucose extracellular concentration detected after SD induction by the small biosensors was lower than that detected by larger ones (135 ± 65 μM versus 293 ± 52 μM, respectively; P = 0.042; n = 7) (Figure 5B2). Furthermore, the time for glucose to return to 80% of its baseline level was 518 ± 72 s according to the small biosensors and 392 ± 54 s according to the large biosensors (P = 0.017; n = 7) (Figure 5B3). Thus, detection of glucose changes in response to SD differed considerably between the implanted small and large biosensors.

Lactate. In addition to glucose, lactate is an important brain metabolite for neurons and glial cells. Levels of extracellular lactate in the brain were monitored with small and large enzyme biosensors that incorporated lactate oxidase. As described above, the two sets of biosensors were implanted *in vivo* 1−2 mm apart. Changes in extracellular lactate were induced by changes in FiO_2[26] and SD. The small biosensors consistently detected a lower lactate concentration: 1.24 ± 0.37 mM versus 2.11 ± 0.85 mM at 100% FiO_2, 2.02 ± 0.60 mM versus 2.78 ± 0.98 mM at 21% FiO_2, and 1.25 ± 0.24 mM versus 1.96 ± 0.36 mM upon return to 100% FiO_2, respectively, in each case (Figure 5C1). Moreover, the differences were statistically significant for the original 100% FiO_2 condition and the return to 100% FiO_2 (P = 0.049, P = 0.013, respectively; n = 7), yet not for the 21% FiO_2 condition (P = 0.156; n = 7).

Smaller changes in the extracellular concentration of lactate evoked by SD were also measured with the small biosensors. SD consistently evoked a wave of increased lactate concentration in the interstitial fluid, consistent with a previous study.[13] The peak lactate concentration and the duration of the increase were not significantly different between large and small biosensors (the maximum lactate increase with conventional biosensors was 10.7 ± 3.8 mM and 10.1 ± 4.1 mM with small biosensors [P = 0.901], and the duration of the increase defined as the time to return to 140% of the baseline lactate concentration was 13.5 ± 2.5 min and 10.1 ± 4.8 min, respectively [P = 0.118]). However, the area under the curve was significantly smaller for the small biosensors, 2.63 ± 0.57 M.s versus 4.34 ± 0.83 M.s for the larger sensors (P = 0.03; n = 7) (Figure 5C2). Thus, monitoring lactate with the minimally invasive microelectrode biosensors resulted in different estimations of lactate concentration compared to the larger devices.

Therefore, the small size of the minimally invasive microelectrode biosensors represented a significant improvement in the ability of microelectrodes to detect interstitial fluid components in the brain, which can be summarized as follows: (1) Probe implantation could be performed without inducing gross tissue deformation or generating cortical SD. (2) The BBB did not exhibit Evans Blue leakage to the brain parenchyma, and glucose diffusion through the BBB was slower, consistent with maintenance of intact blood vessels in proximity of the implanted probes. (3) Basal brain tissue PO_2 and the extracellular concentration of lactate were decreased. (4) Transient neurochemical changes evoked by SD according to the smaller biosensors included reduced lactate release, a greater decrease in glucose level, and larger and faster changes in PO_2.

First-generation oxidase-based microelectrode biosensors, like the ones described here, are dependent on ambient O_2 to catalyze the oxidation of an enzyme substrate and, hence, to detect the molecule of interest. The presence of lower ambient O_2 around small microelectrode biosensors could raise the possibility of O_2 becoming a limiting factor for biosensor functioning, and this could invalidate the concentration estimates provided by these devices. This possibility seems unlikely for our biosensors because during SDs, (1) lactate increased while PO_2 decreased, and (2) PO_2 decreased over 3 min versus over more than 6 min for glucose. Therefore, lactate and glucose concentration changes appear

DOI: 10.1021/acscentsci.8b00797
ACS Cent. Sci. 2018, 4, 1751−1760

to be uncoupled from PO_2 changes, and this supports the dependence of our biosensors on the enzyme substrates, glucose and lactate, rather than ambient O_2.

Overall, the present results support the view that larger probes (e.g., those 80−250 μm in diameter) induce vascular and parenchymal injuries, increase glucose permeability, and are subsequently and rapidly surrounded by a layer of compromised nervous tissue. In addition, decreased O_2 consumption and detection of a higher PO_2 characterize larger oxygen probes. As a result, the interstitial concentrations of neurochemicals in proximity of these larger probes are potentially altered. In contrast, a more intact BBB (indicated with Evans Blue staining) and a slower glucose diffusion rate were observed in proximity of our small microelectrode biosensors. When Ledo et al. implanted a triangular-shaped silicon probe to measure PO_2 in the hippocampus, striatum, and cortex of rats, higher values were obtained in more superficial brain areas in which the probe was wider (e.g., in the cortex, hippocampus area CA1) compared with deeper areas in which O_2 was detected with the tip of the probe (e.g., in the dentate gyrus). These results support the hypothesis that a layer of compromised brain tissue is present along the shaft of larger probes, and O_2 is able to diffuse within this tissue to contribute to the detection of larger PO_2 values. Additionally, faster glucose dynamics, as well as a wider range of glucose variations evoked by SD, are consistent with a layer of inactive cells acting as a low pass filter in the detection of changes in glucose concentration. The higher extracellular concentrations of lactate detected by the larger probes may also reflect the initial stages of an inflammatory reaction toward cells and blood vessels that are injured during implantation. An elevated lactate concentration in the brain has often been associated with brain inflammation, including inflammation induced by AIDS encephalopathy,[27] Leigh syndrome,[28] and inflammatory CNS demyelination.[29] Other laboratories have demonstrated that a layer of compromised brain tissue exists around microdialysis probes and microfabricated silicon probes. For example, 200−500 μm diameter brain microdialysis probes are typically surrounded by compromised tissue, and this impairs dopamine release and the detection of accurate dopamine concentrations.[30,31] In an ultrastructural analysis of brain tissue surrounding a microdialysis probe, neuronal cell death was observed up to 400 μm away from the probe, while tissue disruption including swollen axons and degenerating cell bodies were observed up to 1.2 mm away from the probe.[32] Interleukins, a hallmark of brain tissue inflammation, have also been found to be elevated near microdialysis probes.[33] Meanwhile, similar compromise of brain tissue has been described following the implantation of silicon probes for multisite electrophysiological recordings.[34,35]

Primary injuries that are produced upon brain implantation are believed to be key determinants in the induction of a foreign-body response. This response is initiated by injury to brain capillaries, and it leads to the diffusion of plasma albumin and monocytes to the surface of the implanted device. Eventually, a collagen capsule forms around the probe a few days after implantation.[3] Here, our small microelectrodes had an outer diameter of less than 15 μm, which is the average distance between brain capillaries.[8,20] Thus, this size threshold is considered important to avoid major disruption to the brain parenchyma. Vascular injury is an initial trigger of the foreign-body reaction. Therefore, by reducing vascular disruption it is hypothesized that this foreign-body response could be minimized, and long-term implantation can be achieved. Therefore, it would be of great interest to evaluate the ability of our small microelectrode biosensors to be maintained over several days or longer *in vivo*. Interestingly, carbon fiber microelectrodes have been shown to provide reliable detection of dopamine after several weeks of implantation *in vivo*.[36,37] These results support the hypothesis that small implanted devices achieve greater biocompatibility and longer operational longevity *in vivo*.

In this study, we demonstrated that carbon fiber platinization by physical vapor deposition and subsequent enzyme functionalization can extend the application range of carbon fiber microelectrodes to nonredox molecules, thereby providing minimally invasive microelectrode biosensors less than 15 μm in diameter. We believe these new devices represent a significant advance for neurochemical analyses of brain interstitial fluid and that they will provide improved accuracy in future *in vivo* brain monitoring studies.

■ ASSOCIATED CONTENT

Supporting Information

The Supporting Information is available free of charge on the ACS Publications website at DOI: 10.1021/acscentsci.8b00797.

Additional experimental details and figures including representative cyclic voltammograms (PDF)

Video S1: insertion of a conventional (90 μm diameter) microelectrode biosensor based on a solid Pt/Ir wire into the parietal cortex of an anesthetized rat (AVI)

Video S2: insertion of a 12 μm diameter microelectrode based on a platinized carbon fiber into the parietal cortex of an anesthetized rat (AVI)

■ AUTHOR INFORMATION

Corresponding Author

*E-mail: stephane.marinesco@univ-lyon1.fr.

ORCID

Stephane Marinesco: 0000-0003-2712-6263

Author Contributions

C.C., L.M.-V., and S.M. performed *in vitro* and *in vivo* experiments and analyzed the data. S.M., C.C., and A.M. conceived the study and designed experiments. A.S. and C.C. designed and performed platinization procedures and electron microscopy experiments. S.M. and C.C. wrote the manuscript, with contributions made by all of the other authors.

Notes

The authors declare no competing financial interest.

■ ACKNOWLEDGMENTS

This work was supported by the Foundation Gueules Cassées Sourire Quand Même (FGC49-2016), the CNRS instrumentation aux limites program (BIOSENS15), and Programme Avenir Lyon Saint Etienne (Neurometh), Inserm U1028, CNRS UMR 5292, and University Claude Bernard Lyon I. C.C. is the recipient of a doctoral fellowship from Région Rhône Alpes-Auvergne. We are grateful to Joseph Thumpston and Federica Bellingeri for fabricating and testing biosensors, to Naoufel Haddour for microelectrode characterization, and to Annabelle Bouchardon and the Centre d'imagerie

DOI: 10.1021/acscentsci.8b00797
ACS Cent. Sci. 2018, 4, 1751−1760

quantitative Lyon-Est (CIQLE) at SFR Santé Lyon-Est for the acquisition of microscopy images.

REFERENCES

(1) Bellander, B.-M.; Cantais, E.; Enblad, P.; Hutchinson, P.; Nordström, C.-H.; Robertson, C.; Sahuquillo, J.; Smith, M.; Stocchetti, N.; Ungerstedt, U.; Unterberg, A.; Olsen, N. V. Consensus Meeting on Microdialysis in Neurointensive Care. *Intensive Care Med.* **2004**, *30* (12), 2166−2169.
(2) Jaquins-Gerstl, A.; Michael, A. C. A Review of the Effects of FSCV and Microdialysis Measurements on Dopamine Release in the Surrounding Tissue. *Analyst* **2015**, *140* (11), 3696−3708.
(3) Kozai, T. D. Y.; Jaquins-Gerstl, A. S.; Vazquez, A. L.; Michael, A. C.; Cui, X. T. Brain Tissue Responses to Neural Implants Impact Signal Sensitivity and Intervention Strategies. *ACS Chem. Neurosci.* **2015**, *6* (1), 48−67.
(4) Robinson, D. L.; Hermans, A.; Seipel, A. T.; Wightman, R. M. Monitoring Rapid Chemical Communication in the Brain. *Chem. Rev.* **2008**, *108* (7), 2554−2584.
(5) Wightman, R. M. Probing Cellular Chemistry in Biological Systems with Microelectrodes. *Science (Washington, DC, U. S.)* **2006**, *311* (5767), 1570−1574.
(6) Garris, P. A.; Kilpatrick, M.; Bunin, M. A.; Michael, D.; Walker, Q. D.; Wightman, R. M. Dissociation of Dopamine Release in the Nucleus Accumbens from Intracranial Self-Stimulation. *Nature* **1999**, *398* (6722), 67−69.
(7) Phillips, P. E. M.; Stuber, G. D.; Helen, M. L. A. V.; Wightman, R. M.; Carelli, R. M. Subsecond Dopamine Release Promotes Cocaine Seeking. *Nature* **2003**, *422* (6932), 614−618.
(8) Day, J. J.; Roitman, M. F.; Wightman, R. M.; Carelli, R. M. Associative Learning Mediates Dynamic Shifts in Dopamine Signaling in the Nucleus Accumbens. *Nat. Neurosci.* **2007**, *10* (8), 1020−1028.
(9) Schuvailo, O. N.; Dzyadevych, S. V.; El'skaya, A. V.; Gautier-Sauvigné, S.; Csöregi, E.; Cespuglio, R.; Soldatkin, A. P. Carbon Fibre-Based Microbiosensors for in Vivo Measurements of Acetylcholine and Choline. *Biosens. Bioelectron.* **2005**, *21* (1), 87−94.
(10) Marinesco, S.; Frey, O. Microelectrode Designs for Oxidase-Based Biosensors. In *Microelectrode Biosensors*; Marinesco, S., Dale, N., Eds.; Neuromethods; Humana Press: Totowa, NJ, 2013; Vol. *80* (3 chapter 1), pp 3−25.
(11) Isoaho, N.; Wester, N.; Peltola, E.; Johansson, L.S.; Boronat, A.; Koskinen, J.; Feliu, J.; Climent, V.; Laurila, T. Amorphous Carbon Thin Film Electrodes with Intrinsic Pt-Gradient for Hydrogen Peroxide Detection. *Electrochim. Acta* **2017**, *251*, 60−70.
(12) Dreier, J. P. The Role of Spreading Depression, Spreading Depolarization and Spreading Ischemia in Neurological Disease. *Nat. Med.* **2011**, *17* (4), 439−447.
(13) Balança, B.; Meiller, A.; Bezin, L.; Dreier, J. P.; Marinesco, S.; Lieutaud, T. Altered Hypermetabolic Response to Cortical Spreading Depolarizations after Traumatic Brain Injury in Rats. *J. Cereb. Blood Flow Metab.* **2017**, *37* (5), 1670−1686.
(14) Sanford, A. L.; Morton, S. W.; Whitehouse, K. L.; Oara, H. M.; Lugo-Morales, L. Z.; Roberts, J. G.; Sombers, L. A. Voltammetric Detection of Hydrogen Peroxide at Carbon Fiber Microelectrodes. *Anal. Chem.* **2010**, *82* (12), 5205−5210.
(15) Vasylieva, N.; Marinesco, S.; Barbier, D.; Sabac, A. Silicon/SU8Multi-Electrode Micro-Needle for in Vivo Neurochemical Monitoring. *Biosens. Bioelectron.* **2015**, *72*, 148−155.
(16) Pernot, P.; Mothet, J. P.; Schuvailo, O.; Soldatkin, A.; Pollegioni, L.; Pilone, M.; Cespugijo, R.; Marinesco, S. Characterization of a D-Amino Acid Oxidase Microbiosensor for D-Serine Detection in the Central Nervous System. In *TRANSDUCERS and EUROSENSORS '07—4th International Conference on Solid-State Sensors*; Actuators and Microsystems; IEEE, 2007; pp 99−101.
(17) Malitesta, C.; Palmisano, F.; Torsi, L.; Zambonin, P. G. Glucose Fast-Response Amperometric Sensor Based on Glucose Oxidase Immobilized in an Electropolymerized Poly(o-Phenylenediamine) Film. *Anal. Chem.* **1990**, *62* (24), 2735−2740.
(18) Yu, B.; Long, N.; Moussy, Y.; Moussy, F. A Long-Term Flexible Minimally-Invasive Implantable Glucose Biosensor Based on an Epoxy-Enhanced Polyurethane Membrane. *Biosens. Bioelectron.* **2006**, *21* (12), 2275−2282.
(19) Ohtake, M.; Morino, S.; Kaidoh, T.; Inoué, T. Three-Dimensional Structural Changes in Cerebral Microvessels after Transient Focal Cerebral Ischemia in Rats: Scanning Electron Microscopic Study of Corrosion Casts. *Neuropathology* **2004**, *24* (3), 219−227.
(20) Tsai, P. S.; Kaufhold, J. P.; Blinder, P.; Friedman, B.; Drew, P. J.; Karten, H. J.; Lyden, P. D.; Kleinfeld, D. Correlations of Neuronal and Microvascular Densities in Murine Cortex Revealed by Direct Counting and Colocalization of Nuclei and Vessels. *J. Neurosci.* **2009**, *29* (46), 14553−14570.
(21) Seiffert, E. Lasting Blood-Brain Barrier Disruption Induces Epileptic Focus in the Rat Somatosensory Cortex. *J. Neurosci.* **2004**, *24* (36), 7829−7836.
(22) Saria, A.; Lundberg, J. M. Evans Blue Fluorescence: Quantitative and Morphological Evaluation of Vascular Permeability in Animal Tissues. *J. Neurosci. Methods* **1983**, *8* (1), 41−49.
(23) Ledo, A.; Lourenço, C. F.; Laranjinha, J.; Gerhardt, G. A.; Barbosa, R. M. Combined in Vivo Amperometric Oximetry and Electrophysiology in a Single Sensor: A Tool for Epilepsy Research. *Anal. Chem.* **2017**, *89* (21), 12383−12390.
(24) Hobbs, C. N.; Holzberg, G.; Min, A. S.; Wightman, R. M. Comparison of Spreading Depolarizations in the Motor Cortex and Nucleus Accumbens: Similar Patterns of Oxygen Responses and the Role of Dopamine. *ACS Chem. Neurosci.* **2017**, *8* (11), 2512−2521.
(25) Piilgaard, H.; Lauritzen, M. Persistent Increase in Oxygen Consumption and Impaired Neurovascular Coupling after Spreading Depression in Rat Neocortex. *J. Cereb. Blood Flow Metab.* **2009**, *29* (9), 1517−1527.
(26) Jones, D. A.; Ros, J.; Landolt, H.; Fillenz, M.; Boutelle, M. G. Dynamic Changes in Glucose and Lactate in the Cortex of the Freely Moving Rat Monitored Using Microdialysis. *J. Neurochem.* **2000**, *75* (4), 1703−1708.
(27) Pavlakis, S. G.; Lu, D.; Frank, Y.; Wiznia, A.; Eidelberg, D.; Barnett, T.; Hyman, R. A. Brain Lactate and N-Acetylaspartate in Pediatric AIDS Encephalopathy. *Am. J. Neuroradiol.* **1998**, *19* (2), 383−385.
(28) Detre, J. A.; Wang, Z.; Bogdan, A. R.; Gusnard, D. A.; Bay, C. A.; Bingham, P. M.; Zimmerman, R. A. Regional Variation in Brain Lactate in Leigh Syndrome by Localized 1H Magnetic Resonance Spectroscopy. *Ann. Neurol.* **1991**, *29* (2), 218−221.
(29) Bitsch, A.; Bruhn, H.; Vougioukas, V.; Stringaris, A.; Lassmann, H.; Frahm, J.; Brück, W. Inflammatory CNS Demyelination: Histopathologic Correlation with in Vivo Quantitative Proton MR Spectroscopy. *Am. J. Neuroradiol.* **1999**, *20* (9), 1619−1627.
(30) Borland, L. M.; Shi, G.; Yang, H.; Michael, A. C. Voltammetric Study of Extracellular Dopamine near Microdialysis Probes Acutely Implanted in the Striatum of the Anesthetized Rat. *J. Neurosci. Methods* **2005**, *146* (2), 149−158.
(31) Bungay, P. M.; Newton-Vinson, P.; Isele, W.; Garris, P. A.; Justice, J. B. Microdialysis of Dopamine Interpreted with Quantitative Model Incorporating Probe Implantation Trauma. *J. Neurochem.* **2003**, *86* (4), 932−946.
(32) Clapp-Lilly, K. L.; Roberts, R. C.; Duffy, L. K.; Irons, K. P.; Hu, Y.; Drew, K. L. An Ultrastructural Analysis of Tissue Surrounding a Microdialysis Probe. *J. Neurosci. Methods* **1999**, *90* (2), 129−142.
(33) Woodroofe, M. N.; Sarna, G. S.; Wadhwa, M.; Hayes, G. M.; Loughlin, A. J.; Tinker, A.; Cuzner, M. L. Detection of Interleukin-1 and Interleukin-6 in Adult Rat Brain, Following Mechanical Injury, by in Vivo Microdialysis: Evidence of a Role for Microglia in Cytokine Production. *J. Neuroimmunol.* **1991**, *33* (3), 227−236.
(34) Seymour, J. P.; Kipke, D. R. Neural Probe Design for Reduced Tissue Encapsulation in CNS. *Biomaterials* **2007**, *28* (25), 3594−3607.

DOI: 10.1021/acscentsci.8b00797
ACS Cent. Sci. 2018, 4, 1751−1760

(35) Skousen, J. L.; Merriam, S. M. E.; Srivannavit, O.; Perlin, G.; Wise, K. D.; Tresco, P. A. Reducing Surface Area While Maintaining Implant Penetrating Profile Lowers the Brain Foreign Body Response to Chronically Implanted Planar Silicon Microelectrode Arrays. *Prog. Brain Res.* **2011**, *194*, 167−180.
(36) Clark, J. J.; Sandberg, S. G.; Wanat, M. J.; Gan, J. O.; Horne, E. A.; Hart, A. S.; Akers, C. A.; Parker, J. G.; Willuhn, I.; Martinez, V.; Evans, S. B.; Stella, N.; Phillips, P. E. M. Chronic Microsensors for Longitudinal, Subsecond Dopamine Detection in Behaving Animals. *Nat. Methods* **2010**, *7* (2), 126−129.
(37) Schwerdt, H. N.; Kim, M. J.; Amemori, S.; Homma, D.; Yoshida, T.; Shimazu, H.; Yerramreddy, H.; Karasan, E.; Langer, R.; Graybiel, A. M.; Cima, M. J. Subcellular Probes for Neurochemical Recording from Multiple Brain Sites. *Lab Chip* **2017**, *17* (6), 1104−1115.

DOI: 10.1021/acscentsci.8b00797
ACS Cent. Sci. 2018, 4, 1751−1760